ACS APPLIED MATERIALS & INTERFACES

Research Article

www.acsami.org

Integrating a Semitransparent, Fullerene-Free Organic Solar Cell in Tandem with a $BiVO_4$ Photoanode for Unassisted Solar Water Splitting

Yuelin Peng,[†] Gokul V. Govindaraju,[‡] Dong Ki Lee,[‡] Kyoung-Shin Choi,*[,‡] and Trisha L. Andrew*[,§]

[†]Department of Electrical and Computer Engineering and [‡]Department of Chemistry, University of Wisconsin—Madison, Madison, Wisconsin 53706, United States

[§]Department of Chemistry, University of Massachusetts Amherst, Amherst, Massachusetts 01002, United States

Supporting Information

ABSTRACT: We report an unassisted solar water splitting system powered by a diketopyrrolopyrrole (DPP)-containing semitransparent organic solar cell. Two major merits of this fullerene-free solar cell enable its integration with a $BiVO_4$ photoanode. First is the high open circuit voltage and high fill factor displayed by this single junction solar cell, which yields sufficient power to effect water splitting when serially connected to an appropriate electrode/catalyst. Second, the wavelength-resolved photoaction spectrum of the DPP-based solar cell has minimal overlap with that of the $BiVO_4$ photoanode, thus ensuring that light collection across these two components can be optimized. The latter feature enables a new water splitting device configuration wherein the solar cell is placed first in the path of incident light, before the $BiVO_4$ photoanode, although $BiVO_4$ has a wider bandgap. This configuration is accessed by replacing the reflective top electrode of the standard DPP-based solar cell with a thin metal film and an antireflection layer, thus rendering the solar cell semitransparent. In this configuration, incident light does not travel through the aqueous electrolyte to reach the solar cell or photoanode, and therefore, photon losses due to the scattering of water are reduced. Moreover, this new configuration allows the $BiVO_4$ photoanode to be back-illuminated, i.e., through the $BiVO_4$/back contact interface, which leads to higher photocurrents compared to front illumination. The combination of a semitransparent single-junction solar cell and a $BiVO_4$ photoanode coated with oxygen evolution catalysts in a new device configuration yielded an unassisted solar water splitting system with a solar-to-hydrogen conversion efficiency of 2.2% in water.

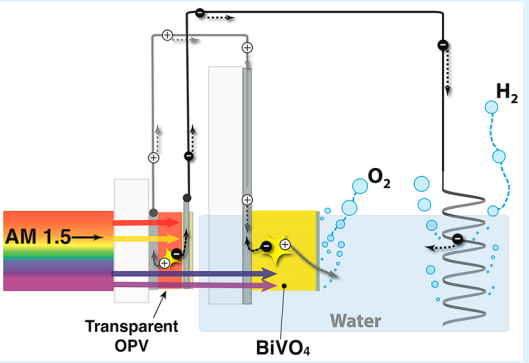

KEYWORDS: *solar fuels, water splitting, non-fullerene acceptor, transparent electrode, bismuth vanadate*

1. INTRODUCTION

Splitting water into H_2 and O_2 using photoelectrochemical cells (PECs) has received significant attention, and vast leaps in materials science and solar-to-hydrogen (STH) conversion efficiencies have been made in the past two decades.[1] PECs are composed of one anode, where water is oxidized to molecular oxygen, and one cathode, where water is reduced to molecular hydrogen. One or both electrodes can be visible light-absorbing semiconductors (photoelectrodes) that generate a photovoltage and directly utilize photogenerated charge carriers for water oxidation or reduction. Bismuth vanadate ($BiVO_4$) has been identified as one of the best photoanode materials due to its low cost, visible light absorption (bandgap 2.4 eV), and favorably positioned valence band edge.[2] The valence band (VB) edge of $BiVO_4$ is located at 2.4 V vs RHE, meaning that photogenerated holes have sufficient energy to oxidize water ($E_{1/2}$ 1.23 V vs RHE). However, the conduction band (CB) edge of $BiVO_4$ is located slightly below 0 V vs RHE, which is the thermodynamic potential for water reduction, and therefore, photogenerated electrons from $BiVO_4$ are not energetic enough for unassisted proton reduction. Nonetheless, the CB edge position of $BiVO_4$ is still the closest to 0 V vs RHE among n-type oxides that can absorb visible light, making $BiVO_4$ the best candidate for the photoanode component of a PEC.[2]

Because of its conduction band edge position, $BiVO_4$-based PECs require extra bias voltage (overpotential) to effect water reduction and achieve water splitting. One approach to provide this necessary overpotential is to serially connect a photovoltaic (PV) cell to the photoelectrode materials.[3] This type of stand-alone device contains multiple light absorbers arising from both the photoanode and photovoltaic components, all of which should, ideally, have complementary absorption profiles to optimize light collection and absorption. Several kinds of PV devices have been employed for stand-alone solar water splitting devices, such as double junction silicon, perovskite, and dye-sensitized solar cells.[1,4−7]

Received: March 29, 2017
Accepted: June 21, 2017
Published: June 21, 2017

DOI: 10.1021/acsami.7b04486
ACS Appl. Mater. Interfaces XXXX, XXX, XXX−XXX

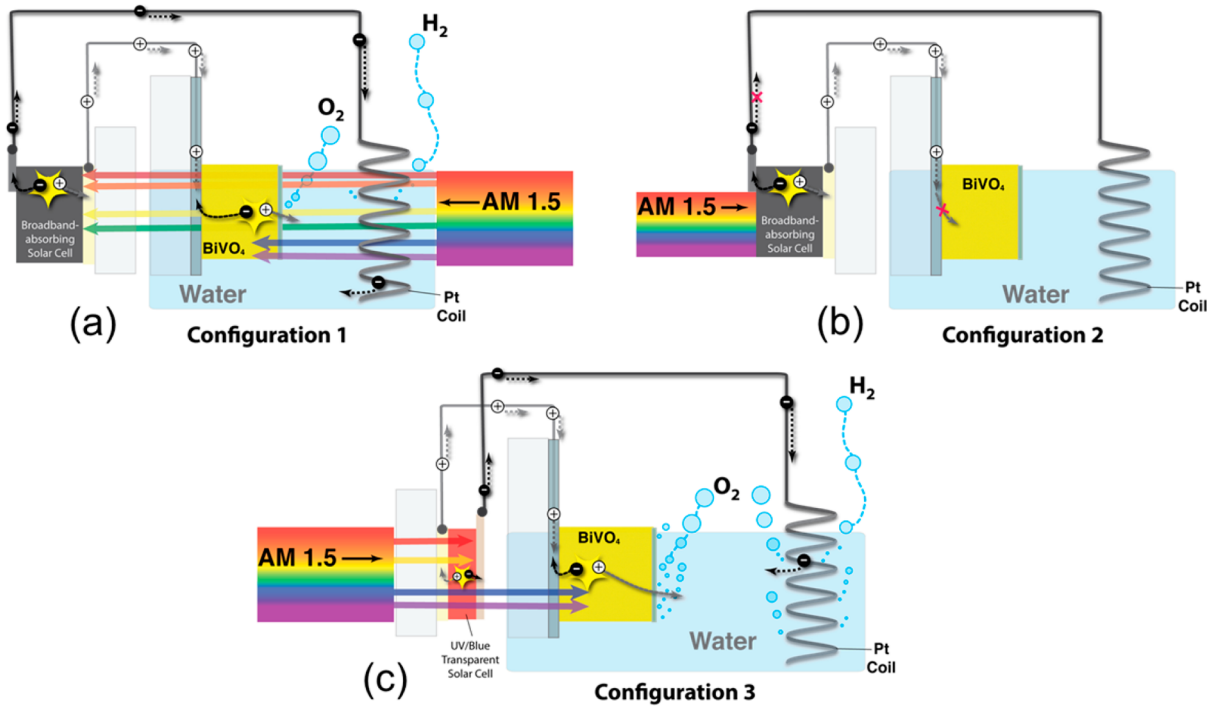

Figure 1. Schematics of three possible configurations of tandem photovoltaic–photoelectrochemical (PV–PEC) cells. (a) Configuration 1, containing a broadband-absorbing PV connected to a $BiVO_4$ PEC. Light must traverse the water bath to front-illuminate the PEC. (b) Configuration 2, containing a broadband-absorbing PV connected to a $BiVO_4$ PEC. Little to no light reaches the PEC. (c) Configuration 3, containing a UV/blue transparent PV connected to a $BiVO_4$ PEC. UV/blue light passes through the PV to back-illuminate the PEC.

All of these previously reported PV/PEC water splitting systems have a similar arrangement of PV and PECs, as Figure 1a illustrates: a cathode is typically placed closest to the light source, followed by the photoanode and then a PV cell (configuration 1, Figure 1a). The reason for this arrangement is that the aforementioned broadband-absorbing PV cells absorb strongly in the same wavelength region as the $BiVO_4$ photoanode. Therefore, the wider-bandgap $BiVO_4$ photoanode must be placed first, in front of the PV, to maximize the total photons utilized by the PV and the $BiVO_4$ photoanode. However, in device configuration 1, solar light must first cross the electrolyte, and therefore the $BiVO_4$ photoanode is front-illuminated (i.e., illumination through the photoelectrode/electrolyte interface) although front illumination of typical undoped $BiVO_4$ electrodes is known to generate lower photocurrents compared to back-illumination (illumination through the $BiVO_4$/transparent back contact) (Figure S1). This is because charge transport in $BiVO_4$ is electron (not hole) transport limited. Back-illumination generates electron–hole pairs near the electron-collecting contact, which allows for more effective separation of electron–hole pairs and optimized charge collection and, thus, higher photocurrents.[9]

A superior arrangement of the PV and PEC components would be to place the PV in front of the $BiVO_4$ photoanode, first in the path of incident light. In this arrangement, incident light passes the solar cell and the $BiVO_4$ photoanode before entering the aqueous electrolyte and the $BiVO_4$ photoanode is back-illuminated, allowing for higher photocurrents. However, if a broadband-absorbing double junction silicon, perovskite, or dye-sensitized PV cell is placed before the $BiVO_4$ (configuration 2, Figure 1b), little to no incident light will pass through the PV component to reach the photoanode. Since the valence bands of most PVs are located above that of $BiVO_4$, photogenerated holes from the PV cannot be injected into the photoanode. This means that a circuit cannot be completed in the absence of $BiVO_4$ photoexcitation. Configuration 2 will only work with a solar cell that is transparent in the 400–510 nm region in which the $BiVO_4$ photoanode absorbs (configuration 3, Figure 1c). These unique requirements led us to investigate the possibility of utilizing organic photovoltaic cells (OPVs) to power $BiVO_4$-based PECs because the localized absorption bands of molecular organic semiconductors allow for fabrication of devices with tunable regions of transparency.[10,11]

Despite the fact that OPVs have been reported to serve as flexible, bandgap-tunable, and potentially transparent solar energy harvesting components in a wide range of applications,[10−15] OPVs have not yet been reported to work as external power sources for solar water splitting PECs containing wide-bandgap oxide photoelectrodes. There are three main reasons for this paucity. First, most OPVs use fullerenes, such as C_{60}, as photoactive electron-transporting materials.[16] Fullerenes and their derivatives display strong absorbance overlap with $BiVO_4$, specifically between 300 and 500 nm, meaning that the OPV and $BiVO_4$ components would compete with each other to absorb incident photons in the 300–500 nm range, reducing the maximum possible solar to hydrogen (STH) conversion efficiency. Second, the open circuit voltage (V_{oc}) of fullerene-based solar cells with high fill factor (FF) is limited to 1.0 V due to the narrow available range of fullerene electronic band edges and bandgaps, which limits the total overall power the solar cell can provide to a serially connected PEC.[17] Third, OPVs have short operation lifetimes compared to inorganic solar cells due to various unavoidable degradation pathways.[18]

DOI: 10.1021/acsami.7b04486
ACS Appl. Mater. Interfaces XXXX, XXX, XXX–XXX

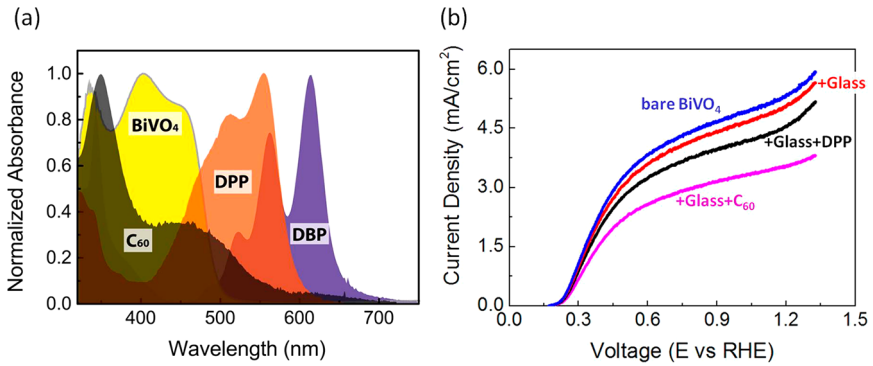

Figure 2. (a) Normalized absorption spectra of DBP, DPP, C_{60}, and the photoanode $BiVO_4$. (b) Photocurrent density−voltage characteristics of a $BiVO_4$ photoanode for sulfite oxidation with different light filters (bare glass, a 20 nm thick DPP film, and a 20 nm thick C_{60} film) placed in front of the $BiVO_4$, in the path of incident light.

Here, we report an unassisted solar water splitting device composed of a $BiVO_4$ photoanode and a stable, non-fullerene, high open-circuit voltage (V_{OC}), single-junction semitransparent organic solar cell. This is the first time a single-junction OPV device is used as an external power supply for a solar water splitting system. In our previous report, we successfully used pyrrolo[3,4-*c*]pyrrole-1,4-dione, 3,6-bis(4-chlorophenyl)-2,5-dihydro (DPP) as a non-fullerene acceptor and tetraphenyldibenzoperiflanthene (DBP) as a donor to produce a high V_{OC}, single junction OPV.[19] By replacing the reflective top electrode with a thin metal film plus an antireflection layer, this solar cell was rendered suitably semitransparent. The major absorption region of this solar cell is complementary to that of $BiVO_4$, allowing for optimized and efficient broadband light collection. In combination with a previously reported nanoporous $BiVO_4$,[20] a heretofore unreported device architecture is provided for the solar water splitting system, which enables back-illumination of the photoelectrode.

2. MATERIALS AND METHODS

Synthesis and Characterization of OPVs. The single-junction OPV used herein was prepared using materials and methods reported in a recent study.[19] DPP was purchased from TCI America, DBP was purchased from Lumtec Corp., and MoO_3, C_{60}, and BCP were purchased from Sigma-Aldrich Company and used without further purification. Organic thin films were grown on 3.5 nm MoO_3 predeposited on indium−tin-oxide coated glass substrate (ITO/glass) under high vacuum ($<10^{-6}$ Torr) at a rate of 0.5 Å/s, with the substrate maintained at room temperature during deposition. DBP:DPP (1:1) blend films were prepared by codeposition with both rates at 0.5 Å/s. Previously optimized photoactive layer thicknesses were used.[19] MoO_3 and the subsequent top-electrode layers were deposited without a mask, while the top Ag or Ag/MoO_3 electrode was deposited with a metal mask to yield a final device area of 3.6 mm^2. Solar cells were then packaged by placing a microscope glass coverslip over the device active area and sealing the edges of the coverslip with a commercial two-part epoxy.

All device-related operation and measurements were performed under ambient atmosphere. Current−voltage characteristics of organic solar cells were measured under dark and simulated AM 1.5G solar illumination from a solar simulator with a Xe-arc lamp. A crystalline Si reference cell was used to measure the intensity of the solar simulator, which was adjusted to 1 sun. Median values of all pertinent OPV device metrics obtained over 20 devices are reported. The optical absorption profiles were obtained by measuring the transmittance and reflectance of the organic films on ITO/glass using an Evolution 220 UV−vis spectrophotometer with ISA 220 integrating sphere.

Synthesis and Characterization of Nanoporous $BiVO_4$ Photoanodes. The nanoporous $BiVO_4$ photoanodes used herein were prepared using the materials and methods reported in a recent study.[20] The surface area and the thickness of the nanoporous $BiVO_4$ photoanode were 31.8 ± 2.3 m^2/g and ~700 nm, respectively. For photoelectrochemical oxidation of water, oxygen evolution catalysts FeOOH and NiOOH were photoelectrochemically deposited on the surface of $BiVO_4$ following the procedures described in the same study.[20] Simulated solar illumination for photoelectrochemical characterization of $BiVO_4$ was obtained by passing light from a 300 W Xe arc lamp through neutral density filters and an AM 1.5G filter. The light then passed through a fused silica fiber-optic cable (Newport Corporation) before illuminating the $BiVO_4$. The light intensity was calibrated to 1 sun using an NREL certified Si reference cell (Photo Emission Tech, Inc.).

Photocurrent density−voltage characteristics of $BiVO_4$ photoanodes for sulfite oxidation were obtained in 0.5 M potassium phosphate buffer (pH 7.3) containing 1.0 M sodium sulfite. Photocurrent density−voltage characteristics of $BiVO_4$/FeOOH/NiOOH photoanodes for water oxidation were obtained in 0.5 M potassium phosphate buffer (pH 7.3) or 1.0 M potassium borate buffer (pH 9.3). The performances of the $BiVO_4$/FeOOH/NiOOH photoanode in these two solutions were comparable, but slightly better long-term stability was observed in borate buffer. The potential was swept from the open circuit potential under illumination to the positive direction with a scan rate of 10 mV/s. All measurements were carried out in a three-electrode configuration using a Pt counter electrode and a Ag/AgCl (4 M KCl) reference electrode, though all results are presented against the reversible hydrogen electrode (RHE) for ease of comparison against the water oxidation and reduction potentials at the specified pH. The potential against Ag/AgCl was converted to that against RHE using the following equation:

$$E\ (\text{vs RHE}) = E\ (\text{vs Ag/AgCl}) + E_{\text{Ag/AgCl}}(\text{reference}) + 0.0591\ \text{V} \times \text{pH} \quad (1)$$

$$(E_{\text{Ag/AgCl}}\ (\text{reference}) = 0.1976\ \text{V vs NHE at 25 °C})$$

Assembly and Characterization of the OPV−$BiVO_4$ System. The OPV was integrated with the $BiVO_4$-based PEC by serially connecting the $BiVO_4$ photoanode to the ITO layer of the OPV and the Pt cathode to the Ag layer of the OPV using silver paste and silver wire (Figure 1c). The system was then illuminated so that the OPV received the 1-sun-calibrated incident light, which then passed through the quartz cell wall and backside-illuminated the $BiVO_4$ electrode. A multimeter (Agilent Technologies, 34401A) was also serially connected to the circuit to measure the output current when the OPV−$BiVO_4$ system was illuminated. The geometric illuminated area of the OPV−$BiVO_4$ system was 0.036 cm^2. To confirm that the photocurrent generated by the OPV−$BiVO_4$ system was truly associated with water splitting, unassisted solar water splitting by the OPV−$BiVO_4$ system was continued for 1 h in an airtight, divided cell where the cathode compartment and the anode compartment were divided by a glass frit. The amount of O_2 evolved was quantified using

DOI: 10.1021/acsami.7b04486
ACS Appl. Mater. Interfaces XXXX, XXX, XXX−XXX

a fluorescence-based oxygen sensor (Ocean Optics, Neofox, FOSPOR-R 1/16 in.) that was placed in the headspace of the airtight cell.[21] The amount of H_2 gas evolved was determined by taking 100 μL of gas from the headspace of the airtight cell using a syringe and injecting it into the gas-sampling loop of a gas chromatograph−mass spectrometer (GCMS-QP2010 Ultra, Shimadzu Corporation) every 20 min. The Faradaic efficiency for gas evolution was calculated by dividing the actual amount of O_2 or H_2 detected by the expected amount of O_2 or H_2 based on the charges from the photocurrent passed through the OPV−$BiVO_4$ system during illumination and then multiplying by 100.

3. RESULTS AND DISCUSSION

Fullerenes, such as C_{60}, are ubiquitous acceptor materials in organic solar cells.[17,22] However, these fullerene-based OPVs are not suitable as external power supplies for water splitting PECs containing $BiVO_4$ photoanode because of detrimental absorption overlap with $BiVO_4$, as discussed earlier. We are therefore required to find a replacement OPV acceptor material that has less absorption overlap with $BiVO_4$ and that yields an OPV capable of generating suitably high power output to effect unassisted water splitting. DPP provides solutions to overcome these challenges and allows integration of an OPV cell with $BiVO_4$ photoanodes to produce a free-standing water splitting device.

The optical properties of DPP and C_{60} were measured, as Figure 2a shows. In contrast to C_{60}, the absorption peaks of DPP were observed at 502 and 548 nm, outside the absorption region of $BiVO_4$. Although DPP also displayed minor absorption bands between 300 and 500 nm, comparatively less light was absorbed by DPP in this wavelength region than by C_{60} (absorption coefficients for DPP and C_{60} are provided in Figure S2). To further investigate the influence of C_{60} and DPP on $BiVO_4$ photocurrents, 20 nm films of C_{60} or DPP were deposited onto glass substrates and placed in front of a $BiVO_4$ electrode, in the path of incident light, and the resulting photocurrent was measured under simulated solar illumination. This setup can be best understood as physically placing a C_{60} or DPP "light filter" in front of the $BiVO_4$ photoanode. Figure 2b shows the effect of various "light filters" on the photocurrent generated by the nanoporous $BiVO_4$ photoanode. The nanoporous $BiVO_4$ electrode used in this study was prepared using a method reported in a recent paper.[20] Photocurrent density−voltage characteristics in Figure 2b were obtained under AM 1.5G (100 mW/cm^2) illumination for sulfite oxidation by the $BiVO_4$ photoanode in a pH 7.3 phosphate buffer solution containing 1.0 M sodium sulfite (Na_2SO_3). Photocurrents for sulfite oxidation instead of water oxidation were measured in this experiment for simplicity; measuring photocurrents for water oxidation using $BiVO_4$ requires placing an oxygen evolution catalyst (OEC) layer on the surface of $BiVO_4$ because $BiVO_4$ is poorly catalytic for water oxidation. In contrast, $BiVO_4$ displays fast oxidation kinetics for sulfite oxidation, and significant photocurrents can be measured without an additional OEC layer.

When a piece of bare glass was placed in front of the $BiVO_4$ photoanode, the photocurrent density at 0.6 V vs RHE dropped from 3.82 to 3.6 mA/cm^2. This decrease was mainly caused by light reflecting off of the bare glass surface before reaching the $BiVO_4$ film. Placing a C_{60} film deposited on the bare glass in front the $BiVO_4$ electrode further reduces the photocurrent density of $BiVO_4$ to 2.57 mA/cm^2 (a 28.6% reduction); however, a DPP film deposited on the bare glass placed in front of the $BiVO_4$ electrode only reduced the photocurrent to 3.3 mA/cm^2 (an 8.3% reduction). These results clearly confirmed that DPP is a superior acceptor material, compared to C_{60}, for OPV cells meant for integration with $BiVO_4$ photoanodes.

The structure of the single junction solar cell used in this work was as follows: glass/ITO 150 nm/molybdenum oxide (MoO_3) 3.5 nm/DBP 5 nm/DBP:DPP(1:1) 30 nm/DPP 5 nm/bathocuproine (BCP) 7.5 nm/top electrode.[19] In order to allow the solar light from 300 to 500 nm, which can be absorbed by $BiVO_4$, to be transmitted through the solar cell and reach the photoanode, the standard reflective top electrode used for most OPV devices had to be replaced by one with high transparency and conductivity. Since the organic layers below the top electrode are soft, thin, and dissolvable in organic solvents, most of the commonly used vapor-deposited and solution-processed transparent electrodes were inappropriate candidates for this work. For example, indium tin oxide (ITO), which is the most commonly used transparent electrode, is not suitable as a top electrode in this particular case because the underlying DBP and DPP layers were found to be damaged during the sputter deposition of ITO. Instead, a thin metal film was investigated as a transparent top electrode due to its high conductivity, good transparency, and benign deposition process.[23] Silver thin films of varying thicknesses were investigated, and a 15 nm thick silver film was revealed to possess the best optical and electrical properties (Figure S3) needed for integration with a $BiVO_4$ PEC.

As Figure 3 shows, the average transmittance value of a 15 nm thick Ag film is 67% in the region from 300 to 500 nm. To further enhance the transmittance of the top electrode of the OPV, a dielectric/metal/dielectric (DMD) structure was used to provide extra small-pass reflectance. BCP served as both the first dielectric layer of the DMD structure and an exciton blocking layer that was in direct contact with the DPP layer. The thickness of the BCP layer used in this DMD electrode was fixed at 7.5 nm, which is the optimal value for solar cell performance.[18] MoO_3 was used as the outer dielectric material of the DMD structure and was used as the antireflection layer to enhance the optical transmittance of the new top electrode.[24] The thickness of the MoO_3 layer was varied from 18 to 23 nm and a slight change of the transmittance peak of the DMD electrode was observed with this thickness variance (Figure 3). Considering the absorbance spectrum of $BiVO_4$, a 20 nm MoO_3 thin film was chosen so that the peak of the DMD transmittance spectrum coincided with the absorption profile of $BiVO_4$. Finally, upon combining a 15 nm thick Ag layer with BCP and MoO_3, the transmittance of the top electrode in the

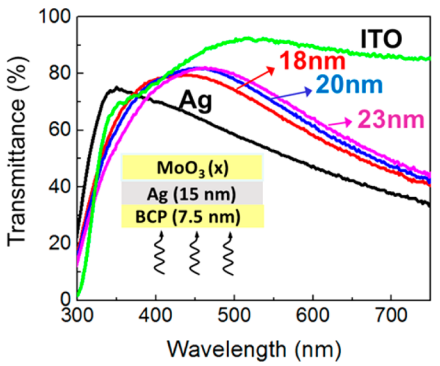

Figure 3. Optical transmittance of BCP/Ag/MoO_3 DMD structures on glass with varying MoO_3 thickness. The transmittance spectra of a 15 nm Ag thin film and ITO on glass are also provided for reference.

DOI: 10.1021/acsami.7b04486
ACS Appl. Mater. Interfaces XXXX, XXX, XXX−XXX

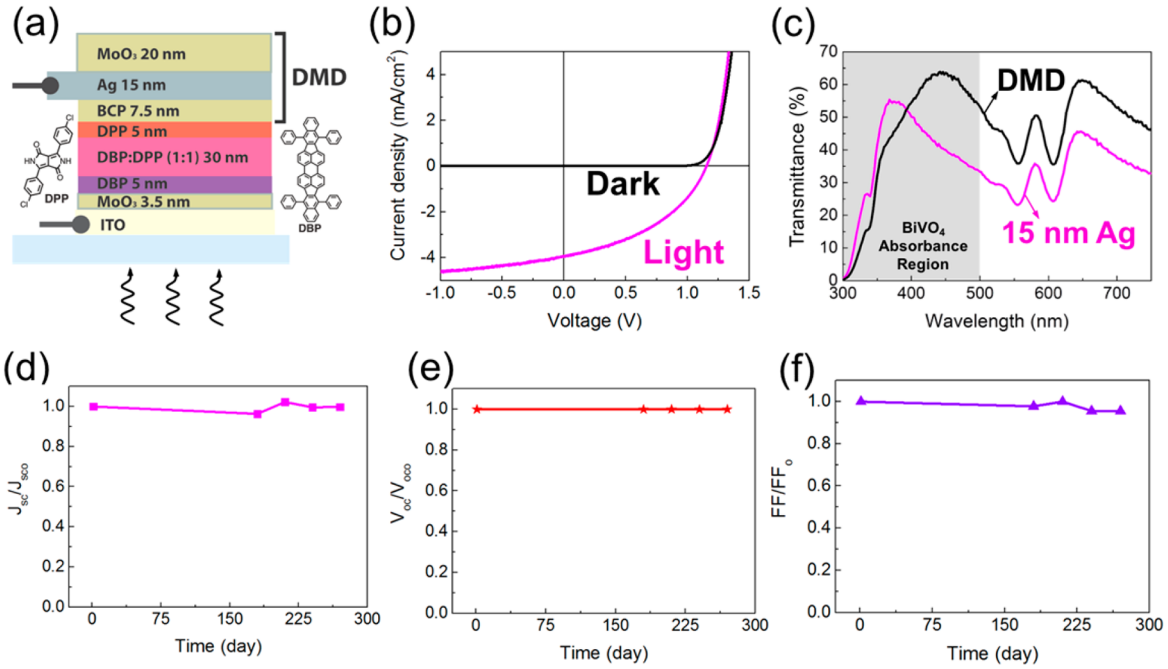

Figure 4. (a) Device structure of the semitransparent single junction solar cell used in this work, including the chemical structures of DBP and DPP. (b) Representative current density−voltage characteristics of the solar cell in the dark and under 1 sun. The device was illuminated through the substrate/ITO. (c) Optical transmittance of the solar cell from (a). The transmittance of an analogous device with only a 15 nm Ag thin film top electrode is provided for reference. (d−f) Stability measurements of the solar cell over 270 days. J_{sc0}, V_{oc0}, and FF_0 are the initial values of J_{sc}, V_{oc}, and FF of the device immediately after fabrication.

wavelength region from 300 to 500 nm efficiently increased to 74%, which is comparable to the transmittance of an ITO electrode as shown in Figure 3. The slight decrease in transmittance from 300 to 370 nm was caused by the absorption bands of BCP and MoO_3 (the absorbance spectra of BCP and MoO_3 are provided in Figure S4). It must be noted that the transmittance of the DMD electrode from 500 to 650 nm was only 66%, which is much lower than the transmittance of an ITO electrode in this wavelength region. However, the intent in using an optically-tunable DMD top electrode was not to globally improve transmittance, but to optimize the reflectance of light between 500 and 650 nm (the region of DBP/DPP solar cell photoactivity), from the top electrode back down to the photoactive layers. By using a DMD electrode, more than 30% of the incident light was reflected back to the photoactive layers of the solar cell and contributed to the photocurrent, whereas very little solar light can be reflected back to the photoactive layers of a solar cell upon using an ITO top electrode.

After combining this DMD top electrode with previously reported photoactive layers[19] and an ITO bottom electrode, a semitransparent solar cell exhibiting a power conversion efficiency (PCE) of 2.04 ± 0.06%, with a V_{oc} of 1.15 ± 0.01 V, a short circuit current density (J_{sc}) of 3.95 ± 0.07 mA/cm^2, and a FF of 0.45 ± 0.02, was obtained (Figure 4a,b). These electrical characteristics are similar to those of the previously reported device containing a reflective silver top electrode.[19] Importantly, the observed maximum power point of the semitransparent single junction solar cell is sufficient to supply enough external power to the $BiVO_4$ photoanode. The transmittance of the solar cell from 330 to 500 nm increased from 43% to 51% by replacing a plain Ag thin film electrode with the DMD electrode as shown in Figure 4c. Further, as expected, the photoactive layers used in this semitransparent solar cell retained their localized photoactivity between 500 and 650 nm (Figure S5), which is outside the absorption region of the $BiVO_4$ photoanode. This organic solar cell also showed notable stability after it was encapsulated with a cover glass and epoxy. We tested the stability of the encapsulated solar cell in air every 30 days after it was initially fabricated for 180 days. As Figure 4d−f shows, the J_{sc}, V_{oc}, and FF values of the solar cell did not significantly change after 270 days of ambient storage under room light.

Before integrating the $BiVO_4$ photoanode and the semitransparent OPV to achieve unassisted solar water splitting, the effect of the OPV in decreasing the intensity of incident light reaching the $BiVO_4$ electrode was first examined by comparing photocurrents for water oxidation with and without placing the OPV in front of the $BiVO_4$ electrode. For this experiment requiring photocurrent measurement for water oxidation, FeOOH and NiOOH were deposited as oxygen evolution catalysts (OECs) on the surface of $BiVO_4$ following a recently published procedure to improve water oxidation kinetics of the $BiVO_4$ photoanode.[20] The photocurrent density−voltage characteristics of the $BiVO_4$/FeOOH/NiOOH electrode for water oxidation were measured in a 1.0 M potassium borate buffer solution (pH 9.3) under AM 1.5G illumination with and without the OPV placed in front of the PEC (Figure 5a). The photocurrent density of $BiVO_4$ at 0.9 V versus RHE was 3.44 mA/cm^2 without the OPV and decreased to 1.76 mA/cm^2 at 0.9 V vs RHE when the OPV was placed in front of the photoanode. This photocurrent decrease was mostly due to the absorption of the solar cell; each layer of the solar cell displayed some absorption overlap with $BiVO_4$ in the region from 300 to 500 nm, which decreased the total photon power incident on the $BiVO_4$ surface. In addition, approximately 6% of the solar light was reflected by the glass substrate of the solar cell, which caused weaker illumination at the surface of the photoanode.

DOI: 10.1021/acsami.7b04486
ACS Appl. Mater. Interfaces XXXX, XXX, XXX−XXX

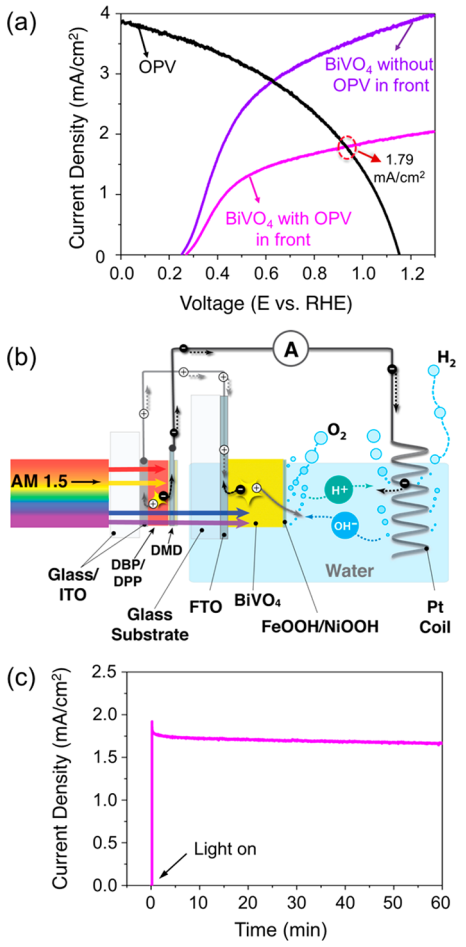

Figure 5. (a) Photocurrent density−voltage characteristics of a $BiVO_4$/FeOOH/NiOOH photoanode for water oxidation with and without the semitransparent OPV in front of the PEC. The photocurrent density−voltage characteristics of the OPV from Figure 4b is overlaid. (b) Schematic of the unassisted solar water splitting device composed of a semitransparent organic solar cell and a $BiVO_4$ photoanode. (c) Photocurrent density versus time plot of the integrated OPV−$BiVO_4$/FeOOH/NiOOH system for unassisted solar water splitting measured in a 1.0 M potassium borate buffer solution (pH 9.3) under AM 1.5G (100 mW/cm^2) illumination.

Figure 5a also shows the photocurrent density−voltage plot of the OPV under 1 sun, which is from Figure 4b, overlaid on top of the photocurrent density−voltage plots of the $BiVO_4$ photoanode for water oxidation. The photocurrent density where the photocurrent density−voltage plot of the OPV and that of the $BiVO_4$ photoanode (with the OPV placed in front $BiVO_4$) intersect is the photocurrent density expected to be generated when these two units are serially integrated to achieve unassisted solar water splitting. The photocurrent density at the intersection point is 1.79 mA/cm^2.

When the OPV and $BiVO_4$ are connected in series, the current flow through each module should be matched so that all the free holes generated in the solar cell can recombine with the free electrons in $BiVO_4$ (Figure 5b).[6−8] The holes generated in $BiVO_4$ are used for water oxidation to O_2 and the electrons generated in the OPV are transferred to the counter electrode for water reduction to H_2. Figure 5c shows the photocurrent density−time plot obtained from the integrated OPV−$BiVO_4$/FeOOH/NiOOH system for unassisted solar water splitting, meaning that other than the photovoltages generated by the OPV and the $BiVO_4$ photoanode, no additional external bias was applied for water splitting. The photocurrent density of 1.79 mA/cm^2 obtained from the integrated system agrees well with the photocurrent density predicted using the intersection point shown in Figure 5a (1.79 mA/cm^2). The photocurrent density generated by the unassisted solar water splitting PEC can be used to calculate solar-to-hydrogen (STH) conversion efficiency using eq 2 assuming 100% Faradaic efficiency for hydrogen production.

$$\text{STH efficiency (\%)} = \frac{|J_{sc}(\text{mA/cm}^2)| \times (1.23\ \text{V}) \times \eta_F}{P_{in}\ (\text{mW/cm}^2)} \times 100 \quad (2)$$

In this equation, J_{sc} is the operating current density, 1.23 V is the thermodynamic potential required for water splitting, and P_{in} is the solar illumination power (1 sun, 100 mW/cm^2). Using eq 2, the STH conversion efficiency achieved by the tandem OPV−$BiVO_4$ PEC system was calculated to be 2.2%. Considering that the photocurrent density at the intersection point is 2.87 mA/cm^2 when the OPV does not interfere with the photon absorption of $BiVO_4$ (Figure 5a), a STH conversion efficiency as high as 3.5% can be theoretically expected, if the transmissivity of the OPV is further optimized. To confirm that the photocurrent generated by the OPV−$BiVO_4$/FeOOH/NiOOH system was truly associated with water splitting, unassisted solar water splitting by the integrated system was performed in an airtight cell for 1 h to quantify H_2 and O_2 gases produced. The results show that the Faradaic efficiency for O_2 production is 90% (Figure S6). The molar ratio of H_2 to O_2 produced was 1.9:1 (Figure S6). The slight deviation from the stoichiometric ratio of 2:1 is due to our imperfect manual sampling method for H_2 for GC-MS analysis, which resulted in a slight loss of H_2 during the analysis.

4. CONCLUSIONS

In summary, a novel device configuration for an unassisted solar water splitting system was demonstrated. In this system, $BiVO_4$ served as the photoanode, and a semitransparent organic solar cell was used as the power supply. This is the first time an organic solar cell was integrated with a $BiVO_4$ photoelectrochemical cell to successfully effect unassisted water splitting. The organic solar cell used in this work has several unique features: (i) DPP was employed as the acceptor material in the organic solar cell, instead of a commonly used fullerene material. The absorption profile of DPP is mostly complementary to that of $BiVO_4$, unlike the largely overlapping absorption profiles of $BiVO_4$ and C_{60}, allowing for optimized light absorption across both device components. (ii) A high V_{oc} of 1.15 V can be achieved by this solar cell with only a single junction structure. This high V_{oc} was advantageous in increasing the maximum power output the solar cell could provide to the photoelectrochemical cell. (iii) A good operation stability was observed for this solar cell. After 270 days, no changes were observed in the values of J_{sc}, V_{oc}, and FF initially recorded for the same solar cell immediately after fabrication. Further, by using a 15 nm thick silver film and an antireflection layer as the top electrode, this solar cell was transformed into a semitransparent device with transmittance of 51% from 330 to 500 nm. This allowed the solar cell to be placed in front of a $BiVO_4$ photoanode and, thus, avoid reduced incident photon flux due to scattering by the aqueous electrolye. In addition, this device configuration (solar cell placed first in the path of light) allowed

DOI: 10.1021/acsami.7b04486
ACS Appl. Mater. Interfaces XXXX, XXX, XXX−XXX

for back-illumination of the $BiVO_4$ photoanode, which is known to lead to higher photocurrents when the charge transport in $BiVO_4$ is limited by electron transport. The new device configuration enabled upon using a semitransparent fullerene-free OPV will increase the flexibility of combining PECs and PVs. Future studies will focus on improving the transmittance of the organic solar cell and reducing reflective losses at various glass/glass and glass/water interfaces. Developing new semitransparent OPVs with a higher J_{sc} or FF can effectively increase the intersect current density circled in Figure 5a, which would also be advantageous.

■ ASSOCIATED CONTENT

Supporting Information

The Supporting Information is available free of charge on the ACS Publications website at DOI: 10.1021/acsami.7b04486.

Absorption coefficients, electrical properties of silver thin films, oxygen/hydrogen gas evolution from the unassisted system (PDF)

■ AUTHOR INFORMATION

Corresponding Authors

*E-mail tandrew@umass.edu (T.L.A.).
*E-mail kschoi@chem.wisc.edu (K.-S.C.).

ORCID

Kyoung-Shin Choi: 0000-0003-1945-8794
Trisha L. Andrew: 0000-0002-8193-2912

Author Contributions

Y.P., G.V.G., and D.K.L. contributed equally.

Funding

Y.P. and T.L.A. acknowledge financial support from the Air Force Office of Scientific Research (Grant FA9550-14-1-0128). G.V.G. and K.-S.C. acknowledge financial support from the National Science Foundation (NSF) under the NSF Center (CHE-1305124) and the Wisconsin MRSEC (DMR-1121288).

Notes

The authors declare no competing financial interest.

■ REFERENCES

(1) Kim, J. H.; Jo, Y.; Kim, J. H.; Jang, J. W.; Kang, H. J.; Lee, Y. H.; Kim, D. S.; Jun, Y.; Lee, J. S. Wireless Solar Water Splitting Device with Robust Cobalt-Catalyzed, Dual-Doped $BiVO_4$ Photoanode and Perovskite Solar Cell in Tandem: A Dual Absorber Artificial Leaf. *ACS Nano* **2015**, *9*, 11820−11829.

(2) Park, Y.; McDonald, K. J.; Choi, K.-S. Progress in Bismuth Vanadate Photoanodes for Use in Solar Water Oxidation. *Chem. Soc. Rev.* **2013**, *42*, 2321−2337.

(3) Walter, M. G.; Warren, E. L.; McKone, J. R.; Boettcher, S. W.; Mi, Q.; Santori, E. A.; Lewis, N. S. Solar Water Splitting Cells. *Chem. Rev.* **2010**, *110*, 6446−6473.

(4) Shi, X.; Zhang, K.; Shin, K.; Ma, M.; Kwon, J.; Choi, I. T.; Kim, J. K.; Kim, H. K.; Wang, D. H.; Park, J. H. Unassisted Photoelectrochemical Water Splitting Beyond 5.7% Solar-to-Hydrogen Conversion Efficiency by a Wireless Monolithic Photoanode/Dye-Sensitized Solar Cell Tandem Device. *Nano Energy* **2015**, *13*, 182−191.

(5) Chen, Y.-S.; Manser, J. S.; Kamat, P. V. All Solution-Processed Lead Halide Perovskite-$BiVO_4$ Tandem Assembly for Photolytic Solar Fuels Production. *J. Am. Chem. Soc.* **2015**, *137*, 974−981.

(6) Abdi, F. F.; Han, L.; Smets, A. H. M.; Zeman, M.; Dam, B.; van de Krol, R. Efficient Solar Water Splitting by Enhanced Charge Separation in a Bismuth Vanadate-Silicon Tandem Photoelectrode. *Nat. Commun.* **2013**, *4*, 2195.

(7) Han, L.; Abdi, F. F.; van de Krol, R.; Liu, R.; Huang, Z.; Lewerenz, H.-J.; Dam, B.; Zeman, M.; Smets, A. H. M. Efficient Water-Splitting Device Based on a Bismuth Vanadate Photoanode and Thin-Film Silicon Solar Cells. *ChemSusChem* **2014**, *7*, 2832−2838.

(8) Kim, J. H.; Jang, J.-W.; Jo, Y. H.; Abdi, F. F.; Lee, Y. H.; van de Krol, R.; Lee, J. S. Hetero-type Dual Photoanodes for Unbiased Solar Water Splitting with Extended Light Harvesting. *Nat. Commun.* **2016**, *7*, 13380.

(9) Zhong, D. K.; Choi, S.; Gamelin, D. R. Near-Complete Suppression of Surface Recombination in Solar Photoelectrolysis by "Co-Pi" Catalyst-Modified W:$BiVO_4$. *J. Am. Chem. Soc.* **2011**, *133*, 18370−18377.

(10) Macko, J. A.; Lunt, R. R.; Osedach, T. P.; Brown, P. R.; Barr, M. C.; Gleason, K. K.; Bulovic, V. Multijunction Organic Photovoltaics with a Broad Spectral Response. *Phys. Chem. Chem. Phys.* **2012**, *14*, 14548−14553.

(11) Cnops, K.; Rand, B. P.; Cheyns, D.; Verreet, B.; Empl, M. A.; Heremans, P. 8.4% Efficient Fullerene-Free Organic Solar Cells Exploiting Long-Range Exciton Energy Transfer. *Nat. Commun.* **2014**, *5*, 3406.

(12) Tang, C. W. Two-Layer Organic Photovoltaic Cell. *Appl. Phys. Lett.* **1986**, *48*, 183.

(13) Xu, T.; Yu, L. How to Design Low Bandgap Polymers for Highly Efficient Organic Solar Cells. *Mater. Today* **2014**, *17*, 11−15.

(14) Lunt, R. R.; Bulovic, V. Transparent, Near-Infrared Organic Photovoltaic Solar Cells for Window and Energy-Scavenging Applications. *Appl. Phys. Lett.* **2011**, *98*, 113305.

(15) Peng, Y.; Zhang, L.; Cheng, N.; Andrew, T. L. ITO-Free Transparent Organic Solar Cell with Distributed Bragg Reflector for Solar Harvesting Windows. *Energies* **2017**, *10*, 707.

(16) Hoke, E. T.; Vandewal, K.; Bartelt, J. A.; Mateker, W. R.; Douglas, J. D.; Noriega, R.; Graham, K. R.; Fréchet, J. M. J.; Salleo, A.; McGehee, M. D. Recombination in Polymer:Fullerene Solar Cells with Open-Circuit Voltages Approaching and Exceeding 1.0 V. *Adv. Energy Mater.* **2013**, *3*, 220−230.

(17) Sauvé, G.; Fernando, R. Beyond Fullerenes: Designing Alternative Molecular Electron Acceptors for Solution-Processable Bulk Heterojunction Organic Photovoltaics. *J. Phys. Chem. Lett.* **2015**, *6*, 3770−3780.

(18) Jørgensen, M.; Norrman, K.; Krebs, F. C. Stability/Degradation of Polymer Solar Cells. *Sol. Energy Mater. Sol. Cells* **2008**, *92*, 686−714.

(19) Peng, Y.; Zhang, L.; Andrew, T. L. High Open-Circuit Voltage, High Fill Factor Single-Junction Organic Solar Cells. *Appl. Phys. Lett.* **2014**, *105*, 083304.

(20) Kim, T. W.; Choi, K.-S. Nanoporous $BiVO_4$ Photoanodes with Dual-Layer Oxygen Evolution Catalysts for Solar Water Splitting. *Science* **2014**, *343*, 990−994.

(21) Govindaraju, G. V.; Wheeler, G. P.; Lee, D.; Choi, K.-S. Methods for Electrochemical Synthesis and Photoelectrochemical Characterization for Photoelectrodes. *Chem. Mater.* **2017**, *29*, 355−370.

(22) Hudhomme, P. An Overview of Molecular Acceptors for Organic Solar Cells. *EPJ. Photovoltaics* **2013**, *4*, 40401.

(23) Shtein, M. Thin Metal Films as Simple Transparent Conductors. *SPIE Newsroom* **2009**, *10*, 1848.

(24) Jung, G. H.; Hong, K.; Dong, W. J.; Kim, S.; Lee, J.-L. BCP/Ag/MoO_3 Transparent Cathodes for Organic Photovoltaics. *Adv. Energy Mater.* **2011**, *1*, 1023−1028.

DOI: 10.1021/acsami.7b04486
ACS Appl. Mater. Interfaces XXXX, XXX, XXX−XXX